Baker NJ, Smith JB, Kulan MC, Turvey S.

Design and Performance of a Segmented Stator Permanent Magnet Alternator for Aerospace.

***IEEE Transactions on Energy Conversion* 2017,**

https://doi.org/10.1109/TEC.2017.2739201

Design and Performance of a Segmented Stator Permanent Magnet Alternator for Aerospace

Nick J. Baker, Daniel J. Smith, Mehmet C. Kulan, Simon Turvey

***Abstract*— In this paper, a permanent magnet alternator which presently relies on magnetic slot wedges is redesigned to give lower iron loss. The new segmented stator design is used as the basis for a validated loss study – comparing bonded lamination stacks with those held together with a punched notch.**

Segmentation is shown to improve the production process, reduce losses and remove the need for wedges, whilst not significantly altering the acoustic performance. In the first series of prototypes, however, where notching is used to secure lamination packs, the process is shown to have adversely affected material properties of the nickel iron laminations and overall measured losses increased. In the second prototype, with thinner laminations and glued stacks, iron loss predictions and measurement agree and are less than the present slot wedge design.

***Index Terms*— permanent magnet alternator, segmented stator, iron loss, aerospace, acoustic noise**

I. Introduction

The use of permanent magnet machines in recent years has risen in transportation applications due to their compactness, lightness and high torque density [1]. The fractional slot concentrated winding (FSCW) machines are key technology for these applications since they are characterized by shorter end winding length, high power density and high fault tolerant capability due to electric, magnetic and thermal separations of the phases [1,2-4]. Nevertheless, FSCW machine are also characterized by excessive rotor eddy current losses circulating in the rotating parts. High spatial harmonic content of the stator magneto-motive force (MMF) and large slot openings are the main reasons of the relevant rotor losses [5,6].

The Permanent Magnet Alternator (PMA) in an aerospace engine provides a redundant power supply to the Full Authority Digital Engine Control (FADEC) engine control electronics and actuators; the PMA is directly driven from the engine gearbox, via a dedicated low speed output and must provide constant power across a wide engine speed range. The power is regulated by the FADEC to a defined output voltage using a fixed frequency PWM shunt. At high engine speeds, the PMA effectively spends much of the time at short circuit to limit the output power. Understanding the 100% speed open and short circuit losses is therefore critical to prevent overheating in service.

There are two key design points. Firstly, the output power must be 50% of rated power at 6% rated speed. This drives the machine size. Secondly, the 100% speed (14,000rpm) short circuit current is limited to prevent overheating. Combined, these design points mean the machine is heavily over rated at 100% speed and requires a high per unit inductance.

The PMA must continue to deliver rated power in one power lane in the event of a fault in any of the other power lanes. Fault tolerance thus requires separation between phases, usually implying single layer fractional slot concentrated winding layout [7].

This work was fully funded by Controls Data Services. Mechanical design, windings and stack assembly was carried out by MTC and AeroStanrew under the SAMULET II Innovate UK funded project.

N. Baker and M. Kulan are with the School of Electrical and Electronic Engineering, Newcastle university, Newcastle, NE1 7RU, UK (nick.baker@newcastle.ac.uk)

D. Smith was with Newcastle University, is now with Dyson, Merz Court, Newcastle, NE1 7RU

S. Turvey is with Rolls-Royce Controls and Data Services, York Road, Hall Green, Birmingham, B28 8LN, UK

Fig. 1. Photograph of incumbent slot wedge design

The present stator design is a conventional stamped single lamination semi-closed slot design with steel slot wedges for mechanical security of the coils and increased inductance. Changing the number of wedges varies the slot leakage and allows manual alteration of the inductance for different requirements without re designing the stamping tool – Fig. 1. [8]

The requirement for high inductance necessitates small slot openings or the use of magnetic wedges [9]. Wedges are a significant source of loss from eddy currents due to their solid magnetically permeable nature, particularly at high speed. Fig. 2 shows the loss distribution of the existing design, as predicted using a 2D FEA package running at short circuit, assuming the wedges were constructed from 0.35mm Silicon Iron laminations. Winding losses are essentially constant throughout, due to the inductance holding down current throughout the speed range. Losses in the wedges account for over one third of the remaining losses – 150 W. Rotor losses are dominated by loss in the retaining sleeve. Reduction in these two sets of losses, and specifically the slot wedges, is the primary driver behind this re-design work.

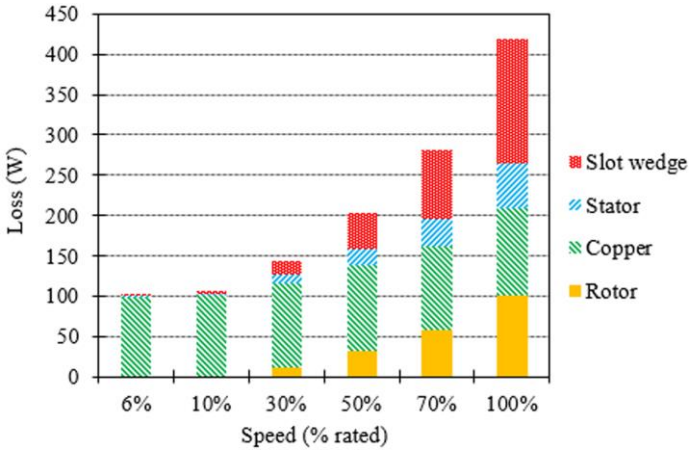

Fig. 2. Short circuit loss distribution of incumbent design.

Heat is removed from the PMA via conduction from the stator housing via the mounting points. Reduction of the iron loss can be assumed to result in a reduction in the operating temperature of the PMA in open circuit. Moreover, by distributing the loss in the tooth tips of the prototype, rather than the wedges of the original design, the thermal path is improved.

Improvement of the manufacturing process, by removing the need for slot wedges or improving the winding method, is the secondary driver of this work. Alternative construction techniques for achieving a high inductance include reduced slot opening, fully closed slot and segmented stator designs. These methods were previously considered with a view to automating the process and allowing for coils to be bobbin wound either directly onto teeth or slid onto teeth as a complete unit [8]. The segmented stator was found to be the most likely to give a reliable automated coil winding, the benefits of such an approach being high copper fill, small end windings and a more reliable manufacturing process.

This paper focuses on the redesign of the PMA to a wedge-free segmented design and considers the impact on machine losses including test results of two prototypes – a bonded lamination stack and one secured via a punched notch.

II. SEGMENTED STATORS

The segmented stator design involves building the machine from single segments consisting of one tooth, Fig. 3. In single tooth wound machines, each segment therefore hosts one coil. Laminations can either be glued together in the normal fashion, or interlocked together by mechanical features such as a punched notch, shown in the left side of Fig. 3. Interlocking requires greater mechanical integrity and hence thicker laminations.

The benefits of segmentation relate to improvements in the winding process. The method will have an impact on thermal behavior, as discussed in [10], and will also likely introduce parasitic air gaps between adjacent segments [11]. The presence of a finite air-gap between stator core segments makes the leakage between tooth tips worthy of consideration [12]. By considering infinitely permeable steel and a reluctance network approach, it has been suggested that the ratio of the reluctance of the joint to the reluctance between stator tips can be used as a design tool to analyze the effect of gaps between stator segments on magnet drive flux leakage. This ratio, α, can be simplified to (1) [12].

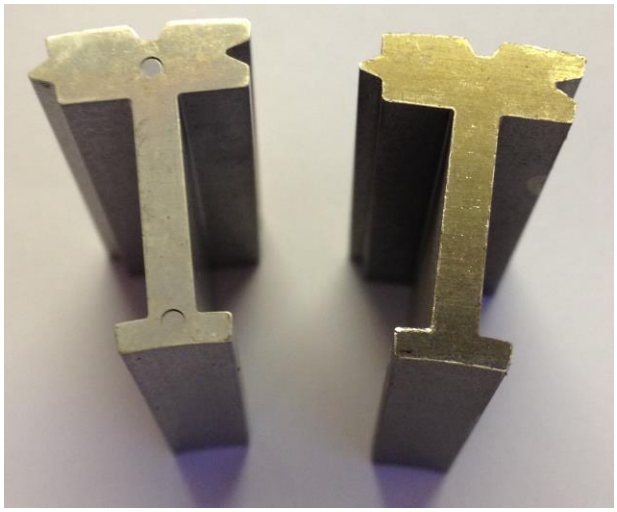

Fig. 3: Single segmented stator tooth. Left hand shows P1, where laminations are locked together by the two visible circular punch marks. Right hand shows P2, where thinner laminations were glued together in the traditional manner.

$$\alpha \approx \frac{g_s}{w_{so}} \times \frac{t_{tt}}{t_{cb}} \qquad (1)$$

Where g_s is the gap between stator segments, t_{tt} is the tooth tip thickness, w_{so} is the width of the stator slot opening and t_{cb} is thickness of the core back.

In the present design, α is 0.0027 for segment gaps of 0.01 mm increasing 20 fold to 0.053 for a 0.2 mm gap. Open circuit back emf will of course reduce linearly with α. Equation (1) can hence be used to estimate a value for g_s if all other parameters are known.

Individual stator segments can be held in place by interlocking, a tension band, or a combination of the two, Fig. 4. It has also been proposed to have fully closed stator slots and have the core back as the segmented component [8,11]. In this work the segments are held in place by a compression band and located by triangle shape features in the core back to minimize pre tension required, Fig. 3.

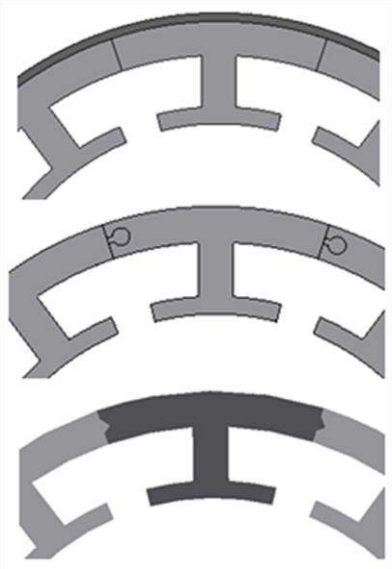

Fig. 4. Alternative methods of locating stator segments: compression ring (upper), fully interlocking (middle) or partially interlocked (lower)

III. Design of the Segmented Stator

A. *Slot Pole Combination*

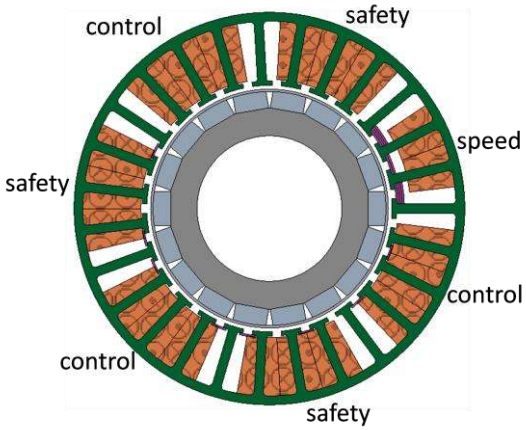

Fig. 5. Original PMA design coil layout.

The PMA design requires four separate three phase power lanes, defined as the 'main' and 'safety' power lanes for channels A and B. Each lane should be physically isolated from the others and there is a requirement for balanced short circuit current across the lanes. Single tooth windings are known to create high spatial harmonics in the air gap magnetic field, so selection of the rotor pole / stator slot combination is critical to the anticipated rotor loss. In the existing design, each of the four three phase power lanes spans two rotor pole pairs. Two independent speed windings occupied a further two pole pairs, giving a 20 pole rotor. The 20 tooth rotor consisted of 12 power lane teeth, 2 speed winding teeth and a further 6 spacer teeth, Fig 5.

During the redesign, external factors required the speed windings to be moved to a separate unit mounted on the end of the rotor. It was hence possible to reduce the rotor to 18 poles. 12 power lane teeth and 6 spacer teeth between each winding gave a 24 stator tooth design.

Simulations showed this design to suffer excessive rotor loss (nearly 500 W) due to a sub-synchronous space harmonic in the air gap, rotating backwards relative to the rotor emanating from the large span of the phase windings. A number of loss reduction techniques were tried, such as a non- conductive rotor sleeve, segmenting the rotor sleeve, eddy current shield, with only limited success and no concept giving less than 200 W of rotor loss. It was concluded that there was no practical solution to limiting the losses of this sub-harmonic, which was a side effect of the tooth/pole number combination.

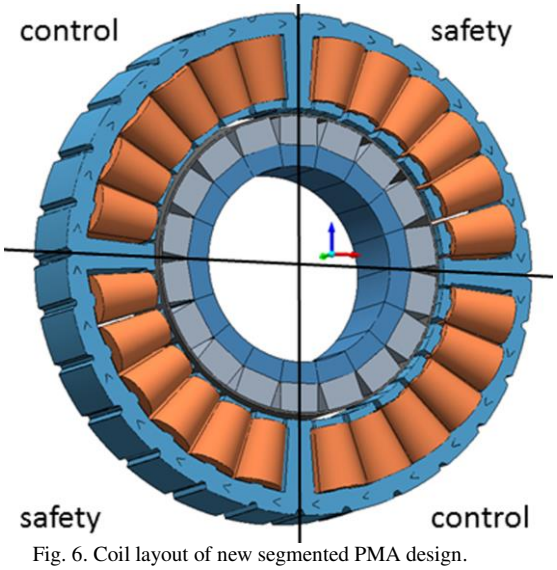

Fig. 6. Coil layout of new segmented PMA design.

After investigating various combinations, an 18 pole rotor was selected. The spacer teeth between power lanes were kept to maintain isolation, and were limited to spanning 2 poles. The four spacer teeth each covered 90^0 electrical between power lanes, totaling 360^0 and leaving 16 poles for the power teeth. The four rotor poles per channel correspond to six 120^0 teeth. The stator therefore has 28 teeth. This removed the sub-harmonic and dramatically reduced the rotor loss. Finally the spacer teeth were thickened up to balance the leakage inductances of the outer coils and in this way the predicted short circuit current imbalance was reduced to 5%.

The final design is shown in Fig. 6, where the four power lanes are defined as the main and safety lanes for channels A and B.

B. Tooth tip

The design process for the PMA focuses on achieving the required back EMF to deliver the low speed power performance, then tuning the inductance to limit the short circuit current at high speed. Reducing current density given a fixed short circuit current requirement tends to require a reduction in turns and a longer machine, as the OD of the stator is fixed. Inductance will be driven by the stator stack length, whereas magnet flux is driven by the axial length of the magnet. The influence of tip geometry on predicted machine inductance was investigated using 3D FEA [8]. Variation of the low current inductance value approximately agreed with the magnitude of α according to the simple relationship (1), until saturation effects become apparent above rated current.

C. Material

The project was advised that the lowest practical thickness of nickel iron is 0.2 mm, which could only be used in traditional round stator bonded or laser welded stacks. For individual interlocking T-sections, designers were advised that to avoid the issues with bonding and laser welding laminations, notched laminations could be used with a minimum thickness of 0.35 mm. This lamination thickness is greater than would normally be used but adequately low losses should be possible if correctly heat treated nickel or cobalt iron is used. To investigate mechanical integrity and losses, Prototype One (P1), used lamination stacks of 0.35 mm held together with notched, whereas Prototype Two (P2) was made from 0.1 mm nickel iron glued stacks, shown in the right hand side of Fig. 3.

IV. Vibration and Acoustic Effects of Segmentation

Electromagnetic forces are the main sources of noise and vibration in PM machines, and acoustics are a known concern with segmentation. In this section the vibration of the segmented and non-segmented stator are compared.

The stress between magnets and armature reaction field is measured as radial force density [13]. According to Maxwell stress tensor method, the radial force in machine airgap can be calculated using [14,15]:

$$F_{rad} = \frac{L_{stk}}{\mu_0} \oint_l (B_n{}^2 - B_t{}^2)\, dl \qquad (2)$$

Where B_n and B_t represents normal and tangential components of flux density in the airgap. L_{stk} is the stack length of PMA and μ_0 is the permeability of vacuum. l is the integration contour line containing stator teeth. If the machine windings are balanced, a net radial force is zero on the stator structure. However, the PMA design developed above could present radial forces on the stator due to the stator structure and pole slot combination. As radial and tangential force density both increase with load, the PMA is investigated at peak current. After determining instantaneous values at different time instants, the average radial pressure acting

on each tooth is calculated as depicted in Fig. 7. This allows the use of a static structural FEA to investigate vibration in the segmented and single component stators.

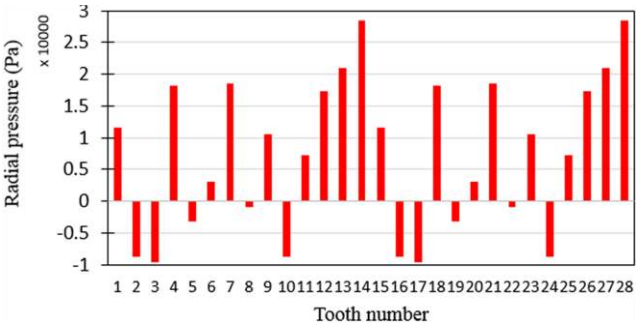

Fig. 7. Radial pressure acting on each tooth of PMA (at load)

The segmented stator is heat shrunk into an aluminum ring, which in the simulation is represented as being fixed from three points 120° apart to predict maximum radial displacement at the outer periphery. Maximum deformation is found to be 0.4 μm for the segmented machine. For the non-segmented stator, total displacement is 0.36 μm showing that the segmented PMA is less rigid than the non-segmented one. Contact faces between the stator segments are treated as bonded and Lagrange based contact formulation was used in Ansys Workbench to obtain contact compatibility between the segments with nearly zero penetration [16]. The peak stress density of the segmented PMA stator obtained from FEA is 1.54 MPa, much less than the yield strength of laminations steels, typically 390 MPa. The structure is thus mechanically sound but could vibrate in the radial direction. As maximum vibration occurs at resonance, the first three natural mode frequency shapes are given in Fig 8. The acoustic properties may now be considered.

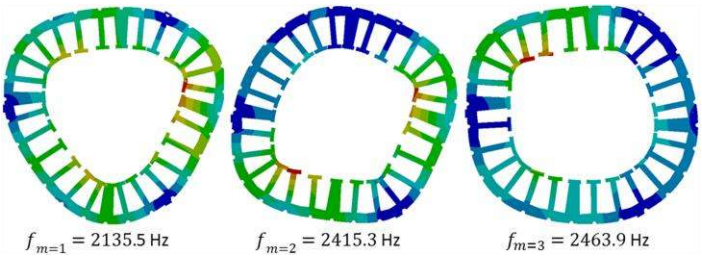

Fig. 8. Mode shapes and eigenvalues for PMA segmented stator

The PMA rotational frequency is 247 Hz and it matches with a 3rd mode frequency about 10 times the excitation. However, the mode frequencies are too high to match with the excitation frequency, f_{exc} of the operating speed. Therefore, the dominant harmonics of the magnetic radial forces cannot excite the machine even in lower order mode shapes.

The acoustic noise can be also determined from the radial displacement, x. The sound power in dB is in the form [17,18]:

$$L_w = 10log\left(\frac{2P_s}{P_{s,ref}}\right) \text{ where } P_{s,ref} = 10^{-12}\,W \qquad (3)$$

The sound power, P_s is given by:

$$P_s = 4\sigma_{rel}\rho c\pi^3 {f_{exc}}^2 x^2 R_{out} L_{stk} \qquad (4)$$

where

$$\sigma_{rel} = \frac{k^2}{1+k^2}\ ;\ k = \frac{2\pi R_{out} f_{exc}}{c}$$

σ_{rel}: relative sound intensity
k : wave number
c: speed of sound (m/s)
ρ : density of air, kg/m^3
R_{out}: stator outer radius, m
L_{stk}: stator stack length, m

By applying (3)-(4), acoustic noise due to maximum radial displacement of the stator structure is predicted to be 51.9 dB for the segmented version and 51.2 dB for the non-segmented version. There is no significant difference in sound levels since maximum radial deflection difference between segmented and non-segmented stator in FEA designs is only is 0.03 μm. Similarly, as coils will not be subjected to increased vibration, it can be assumed that original coil insulation will suffice.

V. Design Validation

A. *Prototypes*

Based on the method and discussion above, a segmented stator was designed, and two prototypes fabricated to be inserted into the existing machine casing. Compared to the existing design, the power requirement was increased and the need for a speed signal from the PMA was removed. Fig. 9 shows P1, prior to insertion in the stator housing with 0.35 mm laminations held together by notching. P1 has a stainless steel compression band. The second prototype, P2, was made from thinner (0.1 mm) nickel iron stacked and glued together with no punch feature.

The prototypes were tested on a constant speed test rig (Fig. 10), where shaft speed, torque and casing temperature were measured.

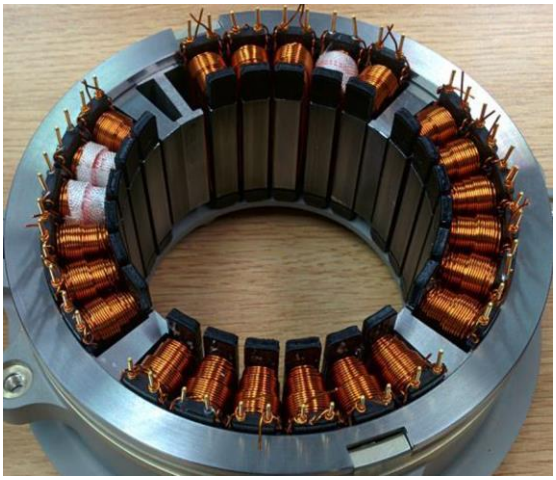

Fig. 9. P1 stator during assembly, prior to inserting in machine casing.

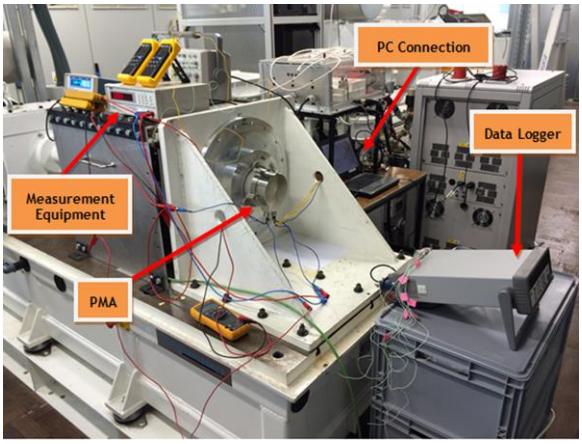

Fig. 10. Machine mounted on test-bed.

B. *Results*

Measured open circuit voltage at 50% speed for P1 is shown in Fig. 11, where a 7% rms over prediction compared to 3D FEA is apparent. The low speed power delivered into a variable load bank by a bridge rectifier connected to two single power lanes is shown in Fig. 12 – showing a power variation of 5% between lanes at peak power.

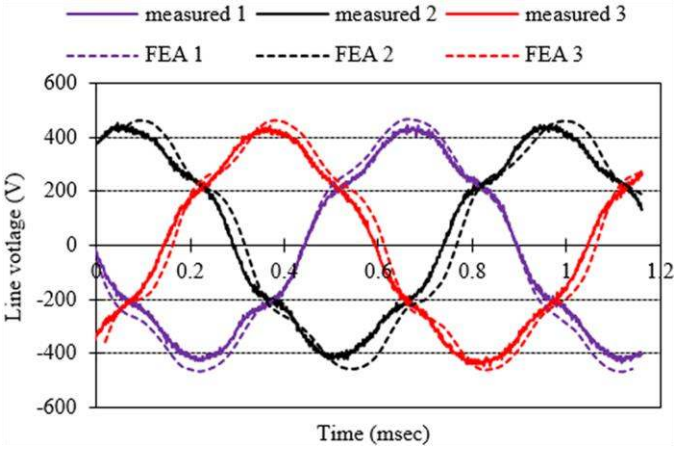

Fig. 11. 50% Speed open circuit back emf results.

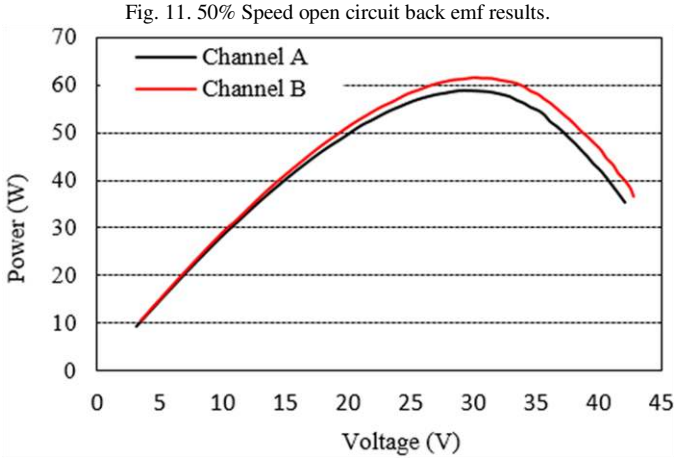

Fig. 12. Power from the DC bus for diametrically opposite power lanes.

From this selection of results, the electromagnetic model is shown to be accurate and consistency between phases is within the required 5%.

VI. Measuring Losses

Two methods were used to independently predict the iron loss: temperature rise and mechanical input power.

A. P1 - Thermal Loss Measurements

Temperature was measured during a 100% speed 90 minutes open circuit test. The temperature of the mounting plate is shown in the solid red line of Fig. 13. The test was repeated with the rotor in air by removing the stator housing – the no-stator test – where the rise of 7.5°C was assumed to be due to bearing loss alone (dotted line Fig. 13). To provide a relationship between temperature rise and total loss, known DC currents were applied across all power coil lanes (grey lines Fig. 13). Assuming a linear relationship between steady state temperature rise and heat energy, equation (5) relates the temperature rise (ΔT) of the base against total power loss for P1. The implied iron loss (open circuit temperature rise minus the no-stator temperature loss) can be deduced to be approximately 420 W during the open circuit test of P1.

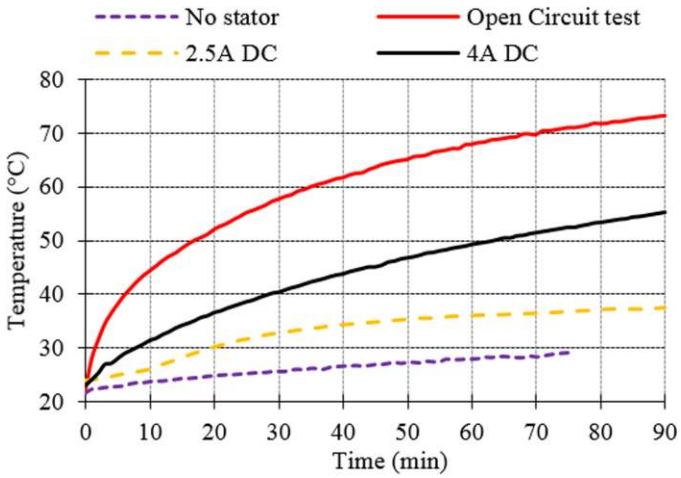

Fig. 13: Base plate temperature variation with time for 100% speed open circuit test and static DC test for reference

$$P_{loss} = \frac{\Delta T}{0.1068} \tag{5}$$

B. P1 - Mechanical Loss Measurements

Mechanical power into the rig is shown in Fig. 14 as measured during the 100% speed open circuit and no stator tests.

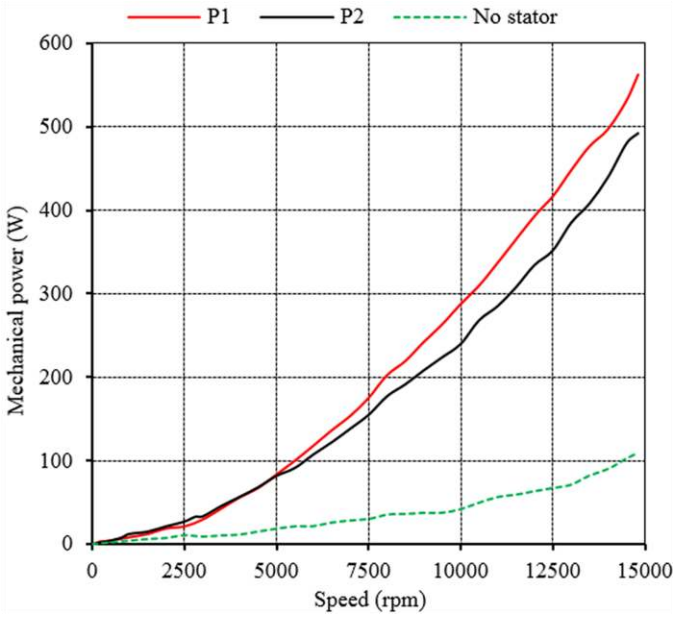

Fig.14. Mechanical power measured during testing of prototype stators P1 and P2, compared to the test with no stator

The total windage and bearing loss during open circuit testing is assumed to be equal to that measured during the no-stator test. Fig. 14 shows the measured value of windage and bearing loss to be large (over 100 W). Bearing and windage loss in the rig is larger than predicted using classical methods – perhaps due to low pre-loading of the bearings or a possible offset in the torque transducer. It is still small compared to the iron loss.

The total mechanical power at 100% speed during open circuit tests of P1 was 560 W, of which the measured windage and bearing losses account for 109 W. The implied iron loss from mechanical power is therefore 563-109=454 W. This and the equivalent value for P2 are given in Table I.

TABLE I
LOSS MEASUREMENTS FOR THE TWO PROTOTYPES

	Thermal method		**Mechanical method**	
	P1	P2	P1	P2
Iron Loss (Watts)	431	354	454	384

C. P2 Measurements

In P2 individual teeth were interference fitted into an aluminum compression ring and mounted in the original housing for mechanical and thermal tests, carried out with no end cap or windings, Fig. 15. The measured mechanical input for the 100% open circuit case was presented in Fig.15 above as 492 W, implying an iron loss of 384 W – a drop of 70 W compared to P1.

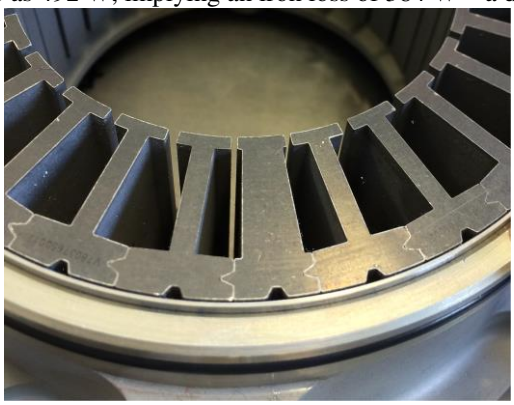

Fig 15. P2 Segments compression fitted into stator housing.

The lack of coils and different compression ring material meant thermal performance differed from that of P1 and prevents the use of the temperature loss relationship given in (5). No coils means it is not possible to repeat the thermal calibration with DC current and provide an updated relationship. Hence, in order to use experimental temperature rise to predict iron loss, a thermal finite element analysis model was adopted to get pseudo experimental results.

A thermal FEA model of P1 was validated by injecting 450 W of iron loss and predicting the temperature rise of the base over a 90 min period. P1 is assembled with a stainless steel compression belt, and the model was adapted to predict temperature increase if the assembly had used an aluminum belt and no windings. By reducing the iron loss injected in to the thermal model until base temperature matched measured experimental value, it has been found that P2 has an iron loss of 354 W.

D. Summary of loss results

The two methods of measuring iron loss give around 70 W less loss in P1 when compared to P2. It is likely that the selection of lamination material (nickel iron) and thickness (0.35 mm), which was driven by the desire for notching in P1, was poor. The introduction of an exotic material, known to be sensitive to manufacturing processes, looks to have been adversely affected by the machining, notching and pre-compression required for this assembly.

E. Annealing the stators

Annealing can be used as a method to recover iron damaged during manufacturing processes, for example it has been reported that annealing the rotor of a switched reluctance machine reduced the iron loss /kg by a factor of 0.62-0.77 [19]. This has not been investigated in this piece of work, but applying this factor to thermally measured loss implies that loss of P2 may be reduced to 219-273 W.

Although comprehensive modeling data was not available for the actual materials used, materials close to the material used in the prototype laminations give a predicted loss of 120 W. This compares favorably with the combined loss of the stator and slot wedges in the existing design.

F. Alternative loss predictions

The experimental figures for iron loss at 100% speed for both prototypes are higher than the predicted iron loss. Four sources of prediction error have been identified and investigated using the transient 3D FEA models shown in Fig 16 to generate the range of loss predictions at 100% speed open circuit, shown in Fig 17. The four loss models are detailed below:

1) Shorted Laminations

The stacking punch used in P1 could be shorting out the laminations providing a path for axial eddy currents. In the FEA model, the notch is modeled as a bar of structural steel running axially though the laminations.

2) Segmentation Gaps

Manufacturing tolerances could result in the presence of small air gaps between adjacent segments. A value of 0.25 mm has been used, being the smallest distance which can be simulated without requiring a prohibitively fine mesh in 3D, and close to the 0.2 mm predicted using equation (1) above.

3) Damaged tooth tips

Material processing is known to damage sensitive materials. Lamination cutting is usually associated with reduced permeability at the edges and could influence the losses [20]. The cutting could also directly distort specific loss density curves, which leads to

higher losses in stator core.

Specifically, it is likely that the loss in the tooth tips - where flux density is the highest and material processing effects most significant compared to the area - is being underestimated. This has been simulated by replacing the material in the tooth tips with one of higher loss properties (M270-35A).

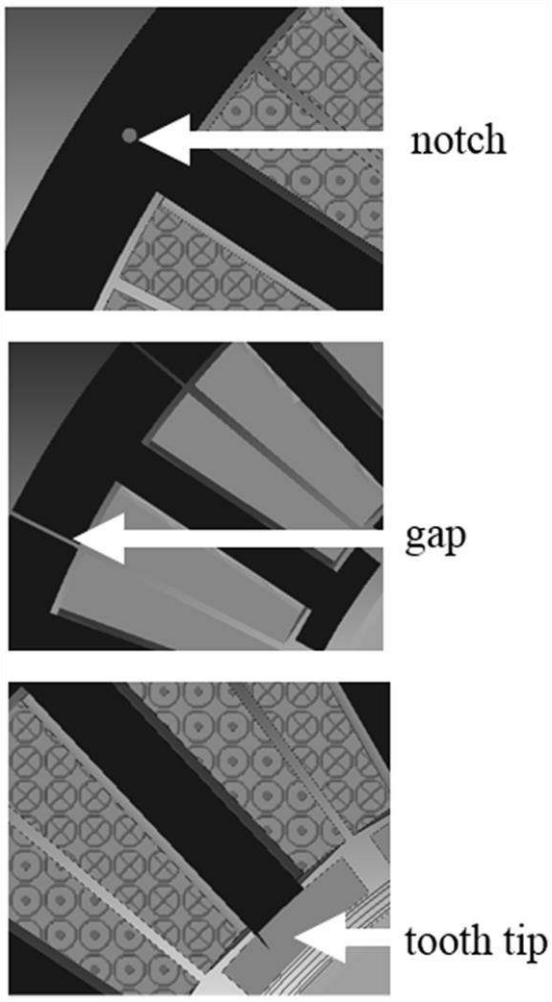

Fig 16. Three simulation scenarios used to investigate losses: (upper) replacing the punched notch with a shorted bar joining laminations; (middle) inserting an air gap between segments and (lower) replacing tooth tips with a higher loss material.

4) Damaged laminations

The effect of material processing on loss properties may not be restricted to the tooth tips with compression and notching effectively damaging the entire stator. Seven alternative core materials have been simulated, from low loss Carpenter 50 to higher loss M270-50A. For P1, the measured value is in fact close to the value predicted assuming regular electric steel (M270-35A).

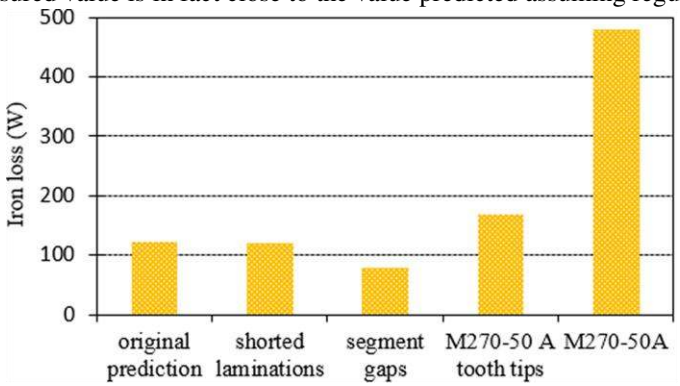

Fig 17. Finite element analysis loss predictions at 100% speed open circuit for the three loss scenarios

G. FEA results

A comparison of the iron loss predicted in the original model and the four alternative scenarios is shown in Fig 17. Shorting the laminations made a negligible impact on losses, whereas the presence of 0.25 mm gaps between segments would reduce loss predictions, due to a decrease in magnitude of flux density in line with equation (1). Simulating material damage in the tooth tips increases loss predictions by around 40%, whereas simulating damage to the whole stator increases losses by a factor of four. This latter prediction matches well with experimental results for P1 and it is reasonable to conclude that in P1 the entire stator material was damaged by notching.

H. Thin Strips

It is well known that punching and cutting laminations has a detrimental effect on the loss properties. In [21] experimental results showed that the iron loss in a 305mm x 30mm strip could be doubled by cutting it into two 15mm strips, and tripled by cutting it into three 10mm strips. This was extrapolated to propose a correction factor which relates iron loss to tooth thickness. In the PMA, the tooth tips are 2mm deep whereas the teeth are 3mm wide. Using (6) from [21] implies a correction factor in the PMA of 1.9-2.4.

$$K = 0.89 + \frac{3}{width} \qquad (6)$$

Applying K to the 120 W FEA loss calculation implies a predicted loss of 228-288W - corresponding well to the measured losses of P2, when corrected for annealing.

VII. Conclusion

A segmented stator design has been presented for a permanent magnet alternator which requires a large per unit inductance. Segmentation was driven by the desire to improve winding reliability and remove the need for manual insertion of loss producing slot wedges. The material choice of nickel iron for a first prototype was governed by the need for 0.35 mm laminations to allow interlocking between laminations. Observed iron loss was found to align with predictions assuming regular electric steel - implying that the entire stator core back material had been damaged during manufacturing. A second prototype, which did not use interlocking was fabricated from thinner nickel iron laminations and found to have 70 W less iron loss at rated speed. By including the effect of annealing in measured results and a build factor relating to the thin aspect ratio of the teeth, loss predictions are matched with experimental data.

Vibration and noise is dependent indirectly on machine electric and magnetic loading combined with the stator structure. It is shown that segmentation does not adversely affect the acoustic behavior in this application.

References

[1] A. Cavagnino, Z. Li, A. Tenconi and S. Vaschetto, "Integrated Generator for More Electric Engine: Design and Testing of a Scaled-Size Prototype," in *IEEE Transactions on Industry Applications*, vol. 49, no. 5, pp. 2034-2043, Sept.-Oct. 2013.

[2] G. J. Atkinson, B. C. Mecrow, A. G. Jack, D. J. Atkinson, P. Sangha, and M. Benarous, "The analysis of losses in high-power fault-tolerant machines for aerospace applications," IEEE Trans. Ind. Appl., vol. 42, no. 5, pp. 1162–1170, Sep./Oct. 2006

[3] A. M. EL-Refaie, "Fractional-Slot Concentrated-Windings Synchronous Permanent Magnet Machines: Opportunities and Challenges," in *IEEE Transactions on Industrial Electronics*, vol. 57, no. 1, pp. 107-121, Jan. 2010.

[4] J. Cros and P. Viarouge, "Synthesis of high performance PM motors with concentrated windings," IEEE Trans. Energy Convers., vol. 17, no. 2, pp. 248–253, Jun. 2002.

[5] D.Maga, M. Zagirnyak, and D.Miljavec, "Additional losses in permanent magnet brushless machines," in Proc. 14th Int. EPE-PEMC, 2010, pp. S4- 12–S4-13.

[6] N. Bianchi, S. Bolognani, and E. Fornasiero, "A general approach to determine the rotor losses in three-phase fractional-slot PM machines," in Proc. IEEE IEMDC, 2007, vol. 1, pp. 634–641.

[7] B.C. Mecrow, A. G. Jack, D. J. Atkinson, S. R. Green, G. J. Atkinson; A. King, B. Green, "Design and testing of a four-phase fault-tolerant permanent-magnet machine for an engine fuel pump", *IEEE Trans. Energy conv.* Vol. 19, 2004, pp 671-678, 2004

[8] N.J. Baker, D. J. Smith, M. C. Kulan, S. Turvey, "Design and performance of a Segmented Stator Permanent Magnet Alternator for Aerospace". In *8th IET International Conference on Power Electronics, Machines and Drives (PEMD 2016)*, Glasgow, 2016

[9] A. Tessarolo, F. Luise, M. Bortolozzi and M. Mezzarobba, "A new magnetic wedge design for enhancing the performance of open-slot electric machines," 2012 Electrical Systems for Aircraft, Railway and Ship Propulsion, Bologna, 2012, pp. 1-5.

[10] R.Wribek, P.H.Mellor, D. Holliday, "Thermal Modeling of a Segmented Stator Winding Design", *IEEE Trans. on Ind. App.* Vol. 47, pp2023-2030, September 2011

[11] Z.Q. Zhu, Z. Azar, G. Ombach, " Influence of Additional Air Gaps Between Stator Segments on Cogging Torque of Permanent-Magnet Machines Having Modular Stators", *IEEE Trans on Magn.*, Vol. 48, pp 2049-2055, June 2012

[12] M. Faizul Momen; S. Datta," Analysis of Flux Leakage in a Segmented Core Brushless Permanent Magnet Motor", *IEEE Trans. on Energy Conv.,* Vol. 24, pp77-81,2009

[13] R. Islam and I. Husain, "Analytical Model for Predicting Noise and Vibration in Permanent-Magnet Synchronous Motors," in *IEEE Transactions on Industry Applications*, vol. 46, no. 6, pp. 2346-2354, Nov.-Dec. 2010.

[14] J. F. Gieras, C. Wang, J. C. Lao, Noise of Polyphase Electric Motors, Taylor & Rancis group, Boca Raton, FL, 2006.

[15] A. Andersson and T. Thiringer, "Electrical machine acoustic noise reduction based on rotor surface modifications," *2016 IEEE Energy Conversion Congress and Exposition (ECCE)*, Milwaukee, WI, 2016, pp. 1-7.

[16] "Ansys Mechanical Structural Nonlinearities – Introduction to Contact" [Online].Available:inside.mines.edu/~apetrell/ENME442/Labs/1301_ENME442_lab6_lecture.pdf
[17] C. Sikder and I. Husain, "Stator vibration and acoustic noise analysis of FSPM for a low-noise design," *2016 IEEE Energy Conversion Congress and Exposition (ECCE)*, Milwaukee, WI, 2016, pp. 1-8.
[18] P. L. Timar, Noise and Vibration of Electric Machines. Oxford, U.K.: Elsevier, 1989.
[19] C. Chiang, A.M. Knight, M. Hsieh, M. Tsai, B.H. Liu, I. Chen, Z. Gaing, M. Tsai, "Effects of Annealing on Magnetic Properties of Electrical Steel and Performances of SRM After Punching", *IEEE Trans. on Magn*., Vol. 50, pp 1 - 4, Nov. 2014
[20] P. Rasilo, U. Aydin, T. P. Holopainen and A. Arkkio, "Analysis of iron losses on the cutting edges of induction motor core laminations," 2016 XXII International Conference on Electrical Machines (ICEM), Lausanne, 2016, pp. 1312-1317.
[21] Y. Liu, S.K. Kashif, A. M. Sohail, "Engineering considerations on additional iron losses due to rotational fields and sheet cutting", in *18th International Conference on Electrical Machines* (ICEM 2008), Vilamoura, 2008

Nick J. Baker received the M.Eng degree in mechanical engineering from Birmingham University, Birmingham, U.K., in 1999, and the Ph.D. in electrical machine design for marine renewable energy devices from Durham University, Durham, U.K., in 2003. He was a Researcher of Machine Design at Durham University in addition to academic posts within Lancaster University's Renewable Energy Group (2005-2008), and currently Newcastle University's Electrical Power Group. He has spent a period in industry as a Senior Consultant for energy consultancy TNEI Services, Ltd., Newcastle, U.K., from 2008 to 2010. He is currently working on machines across the renewable, automotive, and aerospace sectors as a Senior Lecturer.

Daniel J. B. Smith received the MEng in Engineering Economics and Management from Oxford University in 2008 and a PhD from Newcastle University in 2014. His research focus was in high power, high speed electrical machines; defining the coupled electromagnetic, mechanical and thermal limits of performance. He currently works for Dyson Technology Limited as a Senior Engineer researching blue skies electromagnetic systems for future products.

Mehmet C. Kulan received the BSc degree in electrical and electronics engineering from Bilkent University, Ankara, Turkey in 2011 and MSc degree from the University of Newcastle Upon Tyne U.K., in 2013, where he is currently working toward the Ph.D. degree as part of Electrical Power Group, School of Electrical and Electronic Engineering. His research interests include thermal management of electrical machines and finite element modelling of electric machines.

Simon Turvey received an HNC from North Birmingham Poly-Technic in 1976. He is currently working as a specialist engineer in Rolls-Royce Control Systems Research and Technology group where his interests include dedicated electrical machines for gas turbine engines, power conversion and wide bandgap semiconductors.